ORIGINAL PAPER

Tribocorrosion of Pulsed Plasma-Nitrided CoCrMo Implant Alloy

A. Bazzoni · S. Mischler · N. Espallargas

Abstract In the present study, a forged CoCrMo (ISO 5832-12) has been subjected to pulsed plasma treatment in a N_2/H_2 atmosphere at low temperatures (below 500 °C). This treatment resulted in the formation of a layer composed by dispersed chromium nitride particles in a N-enriched metal matrix. The materials were tested for corrosion and tribocorrosion performance in 0.9 wt% NaCl at room temperature under controlled electrochemical conditions. After the treatment, the alloy loses its passive nature. The electrode potential was found to critically affect the corrosion and the tribocorrosion rates. In the nitrided alloy, a significant increase of corrosion rate was found at high potentials, while tribocorrosion was determined mainly by mechanical wear and not affected by potential. On the other hand, the untreated CoCrMo alloy exhibited stable corrosion over a wide range of potentials. Its tribocorrosion rate was similar to the nitrided alloy samples at low potentials, but it increased dramatically at high potentials where passivity triggered severe wear-accelerated corrosion and promoted mechanical wear. The present study shows that the electrochemical conditions determine material deterioration and should therefore be considered when selecting materials for tribocorrosion applications such as biomedical implants.

A. Bazzoni · N. Espallargas (✉)
NTNU, Faculty of Engineering Science and Technology,
Department of Engineering Design and Materials,
Tribology Laboratory, 7491 Trondheim, Norway
e-mail: nuria.espallargas@ntnu.no

A. Bazzoni · S. Mischler
Ecole Polytechnique Fédérale de Lausanne (EPFL),
Tribology and Interfacial Chemistry Group,
Station 12, 1015 Lausanne, Switzerland

1 Introduction

Materials used in biomedical implants include metal alloys, polymers and ceramics, in various combinations. In joint prostheses, these materials are subjected to friction because of the daily activity leading to wear, which considerably shortens the lifetime of the implants in active patients [1]. Furthermore, secondary effects arising from wear are also very important issues. These include biological responses due to released metal ions (mainly in metal implants) and debris (mainly from polymer implants), and the influence of the implant surface on biological tissue, including phagocytosis and biofilm growth. Metals present a unique combination of mechanical, fatigue and chemical resistances, which make them an efficient choice for implants. Indeed CoCrMo self-mated artificial joints are increasingly used in total hip arthroplasty (THA) surgery. Although metal wastage by corrosion and wear is very limited, the long-term accumulation of metal debris in the human body is of great concern. The presence of metal ions in the tissues around hip prostheses has been reported to cause carcinogenicity, hypersensitivity, local tissue toxicity, inflammation and genotoxicity. For instance, Cr^{3+} can cause mutagenesis in the nucleus of the cells [2]. Therefore, methods to reduce material release from CoCrMo alloys implanted in human bodies are sought; in particular, surface treatments have a great technological potential.

In the present study, a pulsed plasma-nitriding process has been selected as surface treatment technique for a biomedical CoCrMo alloy. Nitriding is a surface treatment that allows the diffusion of nitrogen atoms in the surface of

a metal to form a new hard and wear-resistant structure. In the literature, some studies deal with nitriding treatments for biomedical CoCrMo. Wei et al. [3, 4] used a high-intensity plasma ion-nitriding process (HIPIN) to treat CoCrMo at different temperatures. Çelik et al. [5] investigated the effect of the plasma-nitriding temperature and time duration on a CoCrMo alloy, and Pichon et al. [6] investigated the influence of the hydrogen content in the gas mixture and the ion energy using nitrogen implantation on CoCrMo. These studies highlighted the importance of process temperature on the formation of different surface structures on CoCrMo: a hard chromium nitride layer is formed at temperatures above 500 °C, while at temperatures below 500 °C, nitrogen diffuses in the alloy to form a new structure, the so-called γ_N phase, which is a nitrogen-supersaturated fcc structure [7]. The tribocorrosion performance of a plasma-nitrided biomedical CoCrMo alloy at different temperatures has been only studied by Lutz et al. [8] in simulated body fluids. Those authors observed that while nitriding effectively reduces wear in dry conditions, it has a less pronounced or no effect in simulated body fluids depending on process temperature. They observed that material removal proceeds by release of metallic wear particles and of dissolved metal ions due to corrosion. To explain this effect, they proposed that larger process temperatures lead to increased CrN precipitation hardening the alloy but depleting the matrix in Cr with the subsequent loss of passivity. Thus, the overall material loss depends on the balance between corrosion and wear. However, in the said study no experimental evidence or quantitative analysis of this hypothesis was given.

Thus, the aim of the present study is to characterize the tribocorrosion behaviour of pulsed plasma-treated biomedical CoCrMo in simulated body fluid (0.9 wt% NaCl) by quantitatively assessing the contributions of the different mechanical and chemical degradation mechanisms. For this, tests under electrochemical control have been performed at different electrode potentials to simulate different corrosion conditions and to measure in situ and in real-time corrosion kinetics [9]. Chemical analyses of the electrolytes after wear tests were used to quantify the ion dissolution. A tribocorrosion formalism has been applied in the present study to rationalize the involved mechanisms and their quantitative contribution to overall wear.

2 Tribocorrosion Formalism

In a tribocorrosion system, two main mechanisms contribute to overall material loss: the material removal by wear–corrosion interactions from the sliding surface (tribocorrosion) and the corrosion occurring in the overall metal surface exposed to the electrolyte [9]. The different

contributions can be mathematically expressed by the following equations:

$$V_{tot} = V_{tribocorr} + V_{corr} \tag{1}$$

The tribocorrosion component ($V_{tribocorr}$) can be further divided into a mechanical and a chemical component according to

$$V_{tribocorr} = V_{mech} + V_{wac}, \tag{2}$$

where V_{tot} is the overall volume loss from the sample including the material removed from the sliding surface by mechanical wear (V_{mech}) and wear-accelerated corrosion (V_{wac}) as well as the material removed by corrosion inside and outside the wear track (V_{corr}). V_{mech} is the equivalent metal volume ejected from the contact as metal particles. Wear-accelerated corrosion (V_{wac}) arises from the cyclic depassivation and repassivation processes occurring during rubbing within the wear track [9]. This process manifests itself in tests under applied passive potential by an increase in current at the onset of rubbing. This excess current disappears at the end of rubbing when depassivation ceases.

The corrosion volume (V_{corr}) is described by Eq. 3, where v_{corr} is the corrosion rate on the overall electrode (mm/s), A is the area (mm^2) of the electrode exposed to the electrolyte and t is the duration of the experiment (s).

$$V_{corr} = v_{corr} A t \tag{3}$$

In typical laboratory tribocorrosion tests, flat surfaces are rubbed against a smaller counterbody forming a wear track. The wear track volume is usually quantified by profilometry taking the unrubbed surface surrounding it as reference plane. Thus, the wear track volume ($V_{wear\ track}$) corresponds to $V_{tribocorr}$. In tests at applied passive potential, the V_{wac} volume can be calculated by integrating the excess current over the rubbing time and converting it into material loss using Faraday's law [9]. The corrosion rate v_{corr} is proportional to the electrochemical current density i. At the open circuit potential (OCP), the corrosion current density i_{corr} can be extracted from polarization curves using Tafel extrapolation or by determining the polarization resistance. At the applied anodic potentials, the corrosion rate (v_{corr}) corresponds to the measured current provided that metal dissolution is the dominating electrochemical reaction.

3 Experimental Set-Up

The metal used in this study was a forged Co28Cr6Mo alloy (ISO 5832-12 [10]), with the composition as shown in Table 1.

For all experiments, disc samples with thicknesses of 5 mm were cut from rods. The samples were ground and polished until reaching a mirror-like surface finishing.

Table 1 Chemical composition of the alloy

Element	Co	Cr	Mo	Fe	Mn	Si	C	Ni	N
Wt%	Balance	27.7	5.7	0.17	0.8	0.4	0.04	0.3	0.16

Before the nitriding process and the electrochemical and tribological tests, the samples were cleaned in water, rinsed in ethanol and dried in air.

Two different pulsed plasma-nitriding treatments were performed at two different temperatures (350 and 450 °C). The gas composition, voltage and treatment time remained constant. The nitrided samples will be referred as PPN-I (350 °C) and PPN-II (450 °C) hereafter. The microstructures of the layers were studied by X-Ray diffraction (XRD) D8 Focus from Bruker AXS, LynxEye detector (K_α(Cu) = 1.54 Å; 40 kV; 30 mA). The surface and cross-sectional microhardnesses were determined by Vickers indentation (each measurement was performed at least five times).

The corrosion resistance was evaluated by means of polarization measurements in aerated and unstirred 0.9 wt% NaCl, which is close to the saline composition of the body fluids. For these experiments, a previously described electrochemical cell was used [11]. An Ag/AgCl/KCl$_{sat}$ electrode [potential of which with respect to the standard hydrogen electrode (SHE) is 0.196 V] was used as reference electrode, and the auxiliary electrode was a Pt wire. For the convenience of the reader, all the potentials in this article are given with respect to the SHE. A working electrode of each sample was fixed at the bottom of the electrochemical cell, exposing an area of 0.78 cm^2 to the solution. After the stabilization of the OCP, the polarization curves were recorded dynamically using an Autolab PGSTAT 302N Potentiostat at a scan rate of 0.5 mV s^{-1} in a potential range from −1.2 to +1 V$_{SHE}$. Each measurement was carried out two times to check the repeatability of the experiments.

The tribocorrosion of the materials was evaluated in a reciprocating tribocorrosion equipment described in detail elsewhere [12]. The sliding was established by rubbing an alumina ball of 4.76-mm diameter against the samples, which were immersed in the solution. A set of potentiostatic tests was carried out at one cathodic potential (−1.2 V$_{SHE}$) and one anodic potential (+0.5 V$_{SHE}$), which were selected from the recorded polarization curves. A test at OCP was also performed. A potentiostat (Gamry Series G300) was used to control the potential of the samples during the potentiostatic tribocorrosion tests. The reference electrode used was a Ag/AgCl/KCl$_{sat}$ electrode, and the auxiliary electrode was a Pt wire. The ball was driven with a stroke length of 10 mm and an average oscillation frequency of 1 Hz for an imposed number of 3,600 oscillation cycles. The normal force used (10 N) corresponded to an average Hertzian pressure of 4,200 MPa. This value is higher than the yield strength of the alloy (890 MPa [13]), and the test conditions do not correspond to the pressure during human activity, which is lower than 20 MPa [14]. However, this high pressure permits to accelerate tests. Each measurement was carried out two times with new alumina balls to check the repeatability of the experiments. The potentiostatic tests consisted of four steps: (1) stabilization of the OCP during 10 min, (2) application of the selected potential during 5 min, (3) rubbing under applied potential during 60 min and (4) standby at the OCP after rubbing during 10 min. During steps (2)–(4), the current and the frictional force were continuously monitored. The tests at OCP consisted of steps (1), (3) and (4), with the potential and the frictional force being continuously monitored. Sliding tests at dry conditions were also performed at normal load of 10 N against alumina ball of 4.76-mm diameter.

The volume of the wear tracks was quantified by means of confocal microscopy (IFM Alicona instrument). The cross-sectional profiles were taken across the wear track for each sample at one-fourth, one-half and three-fourths of the stroke length. The total volume loss was obtained by multiplying the average area of the cross-sectional profiles by the stroke length.

The microstructure of the wear tracks was studied using a Scanning Electron Microscope (SEM) from Hitachi S-3400N.

The ion concentration of the electrolyte solutions after the tribocorrosion tests was measured using Inductively Coupled Plasma-Mass Spectroscopy (ICP-MS Finnigan Element 2 instrument). For this, the solutions of the two repetitions of each tribocorrosion test were retrieved by pouring the cell content into the same plastic container, then mixed, diluted and digested with 20 % v/v HNO$_3$.

4 Results

4.1 Structural Characterization

The thickness of the nitriding-affected zone was estimated to be between 4 and 5 μm from metallographic cross sections analysed using Backscattered Scanning Electron microscopy (BSE) and shown in Fig. 1.

Figure 2 shows the XRD spectra of the untreated CoCrMo alloy, PPN-I (350 °C) and PPN-II (450 °C) samples. The untreated alloy exhibits the peaks labelled as

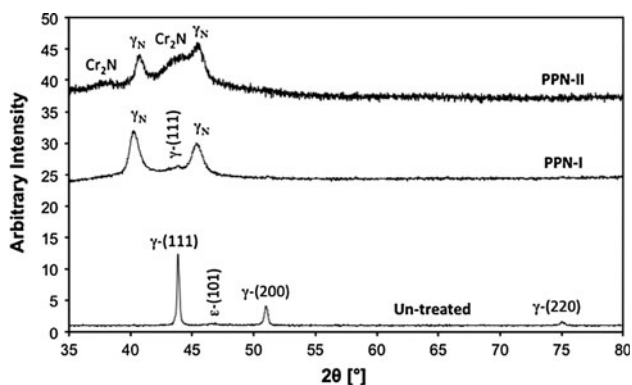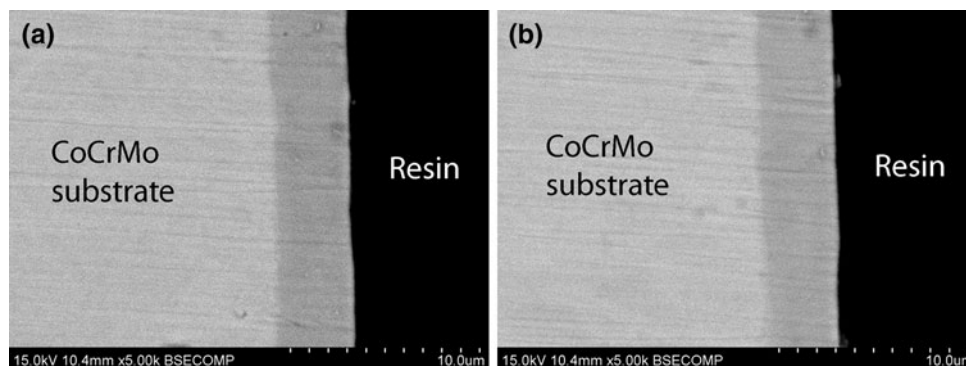Fig. 1 Cross-sectional SEM pictures of **a** PPN-I and **b** PPN-II treatments

Fig. 2 XRD spectra of the untreated, PPN-I and PPN-II samples

γ-(hkl) for the face centred cubic (fcc) phase and ε-(hkl) for the hexagonal close packed (hcp) phase. After the treatments, two new and broad peaks at 40.5° and 45.5° appear in the spectra of the treated samples (Fig. 2). These peaks are characteristic of the nitrogen occupying octahedral interstitial sites in supersaturated phase (γ_N), which is an expanded structure of the γ phase. This phase has been also found in nitrided austenitic stainless steels and CoCrMo [4–7]. For PPN-II, besides the γ_N phase, two broad peaks at 38° and 45° are observed, the first one corresponding to CrN [5] and the second to Cr_2N [4]. This leads to a Cr depletion of the metal matrix. The broad shape of the CrN/Cr_2N peaks indicates that these phases are in the form of nanocrystalline/amorphous precipitates. In the case of PPN-I there is no evidence of chromium nitride precipitates.

The temperature at which the γ_N phase forms in CoCrMo alloys is not commonly agreed in the literature [3–7, 15]. The lowest temperature of γ_N formation has been found by Lutz et al. [15] at 230 °C during plasma immersion ion implantation of CoCr alloys, having its maximum at 370 °C. This last value is not far from the lowest temperature (350 °C) of pulse plasma nitriding investigated in this article (PPN-I) at which a maximum intensity of the γ_N peaks has been found.

The Vickers microhardness measured by indentation at the surface increased from 400 $HV_{0.1}$ (untreated CoCrMo

alloy) to 800 $HV_{0.1}$ for PPN-I and 950 $HV_{0.1}$ for PPN-II. The Vickers microhardness of the nitrided layers as measured on cross-sections was 800 $HV_{0.01}$ and 1,000 $HV_{0.01}$ for PPN-I and PPN-II, respectively.

4.2 Polarization Behaviour

Figure 3 shows the polarization curves obtained in 0.9 wt% NaCl for all samples. For clarity only the potentials from −0.55 to 1 V are plotted in the polarization curves presented in Fig. 3. For the untreated sample four well defined regions can be observed: the cathodic domain (potential below E_{corr}), the cathodic-anodic transition at E_{corr}, the passive plateau (between +0.1 and +0.8 V) and the transpassive region (above +0.8 V). In the cathodic domain, no corrosion occurs, and the current measured is negative because of the reduction of oxygen and water, the latter reaction leading to hydrogen evolution at potentials below −0.5 V. During the cathodic-anodic transition the recorded current goes through zero. In the passive plateau the build up of a protective surface oxide film limits the current in the passive plateau to a value lower than 1 μA/cm^2. At high anodic potentials (>+0.8 V), transpassive dissolution is observed: the current increases abruptly
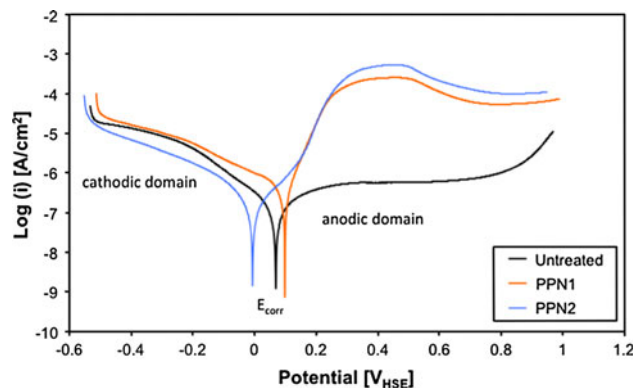

Fig. 3 Polarization *curves* of untreated and treated CoCrMo in 0.9 % NaCl. As the two repetitions of the tests overlapped well, only one *curve* is plotted for clarity

Table 2 Corrosion current densities and potentials

	i_{corr} (µA/cm^2)	E_{corr} (V)
Untreated CoCrMo alloy	0.05	0.087
	0.06	0.057
PPN-I	0.49	0.074
	0.45	0.099
PPN-II	0.14	−0.009
	0.06	−0.005

The results of two independent experiments per each testing condition are shown in the table

because of the oxidation of water and of the passive film [16].

After nitriding, the samples exhibit a different polarization behaviour. While the cathodic domain is similar to the untreated alloy, the anodic domain is characterized by much higher current densities suggesting absence of passivity. Apparently the loss of passivity is a consequence of the formation of the γ_N phase rather than the depletion in Cr due to nitrides formation as usually indicated in literature [8]. Indeed, PPN-I and PPN-II behave similarly although chromium nitrides form predominantly in PPN-II as confirmed by the XRD results. The corrosion rates listed in Table 2 were calculated by measuring the polarization resistance at the corrosion potential and converting them using Stern-Geary approximation (the anodic and cathodic Tafel coefficients were assumed to be 50 mV).

4.3 Tribocorrosion Behaviour

Figure 4 shows the evolution of the coefficient of friction (COF) with time during tribocorrosion tests performed at OCP for the untreated alloy. A similar behaviour was observed independently on surface treatment, potential and the presence or the absence of electrolyte. In Fig. 4, the COF attains rapidly a steady-state value and exhibits relatively large noise, which for this tribometer is usually
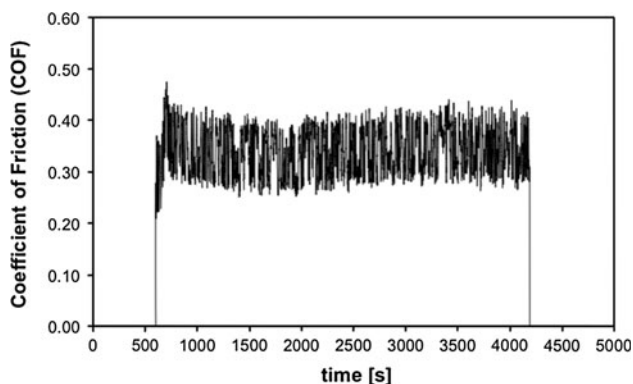
associated to the presence of debris within the contact. Indeed, the behaviour of third-body particles was found to critically affect friction in the tribocorrosion of CoCr alloys [17]. For comparison purposes, the COF values averaged during the entire rubbing period are listed in Table 2. No significant variation of the COF occurs with potential or material.

Figure 5 shows the evolution of OCP with time for all samples. At the onset of rubbing, the potential of the untreated CoCrMo alloy shifted to more cathodic values. Such a drop in potential is usually observed in passive metals [9] when the layer of the alloy is locally removed by friction, and as a consequence, a potential difference is established between depassivated areas (anodic) and still passive areas (cathodic). Thus, the potential drop reflects the extent of depassivation caused by the sliding ball. For the untreated CoCrMo sample, the recovery of the potential, after the rubbing stops, takes a finite time.

The nitrided samples exhibit a different OCP behaviour during rubbing. In the case of PPN-II, the onset of rubbing corresponds to an initial short decay of the potential followed by a peak after which the potential increases steadily until the end of the test and recovers the pre-rubbing value. The PPN-I sample shows an intermediate behaviour between the untreated alloy and the PPN-II sample. At the beginning of the test, an initial drop in potential is observed, followed by a peak and a plateau where the potential remains lower than the initial OCP value. After the rubbing stops, the potential immediately is restored to the initial OCP value. This suggests that PPN-I is passive at OCP.

The evolution of current during potentiostatic tribocorrosion tests at +0.5 V is shown in Fig. 6. In the case of the untreated CoCrMo sample, the current increases up to a value of 0.13 mA (Table 3) under the action of rubbing. This effect is due to the passive film removal and the metal dissolution occurring inside the wear track [9]. When the

Fig. 4 COF evolution with time during the tribocorrosion tests at OCP of PPN-I sample in 0.9 wt% NaCl
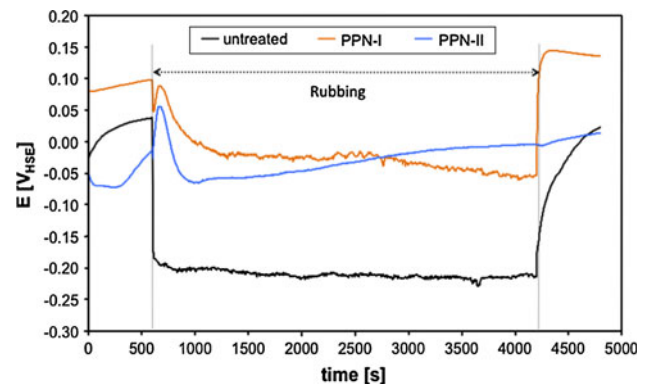

Fig. 5 Potential evolution with time during the tribocorrosion tests at OCP of treated and untreated samples in 0.9 wt% NaCl. Only one *curve* of each test is shown for clarity
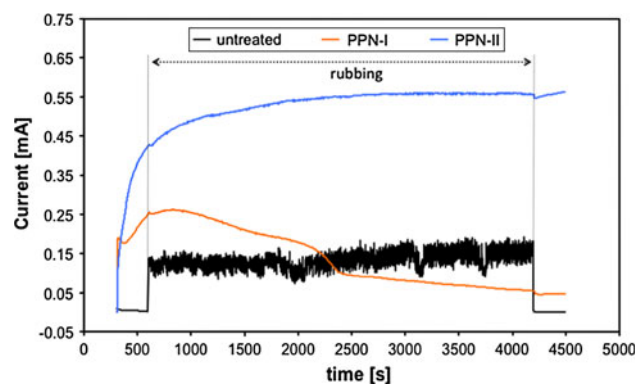
Fig. 6 Current evolution with time for tribocorrosion tests of treated and untreated samples in 0.9 wt% NaCl at +0.5 V. Only one *curve* of each test is shown for clarity
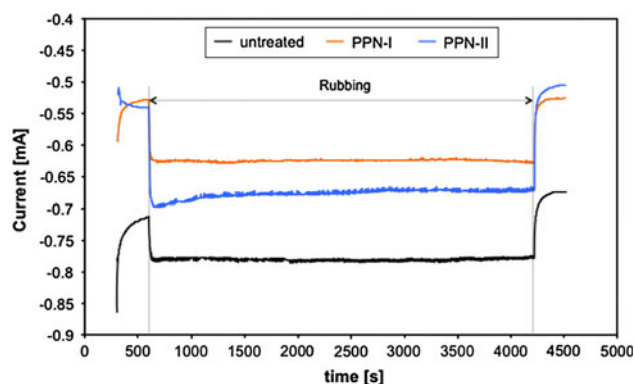

Fig. 7 Current evolution with time for tribocorrosion tests of treated and untreated samples in 0.9 wt% NaCl at −1.2 V. Only one *curve* of each test is shown for clarity

rubbing stops the recorded current decreases to the value established before rubbing started (~ 0 mA) indicating the restoration of passivity [9]. In the case of the nitrided samples the current before rubbing is much higher than for the untreated passive alloy. This is in agreement with the polarization curves. Rubbing did not have any effect on current confirming the absence of passivity already observed in the polarization curves.

The effect of rubbing on the cathodic current is quite similar for all samples (Fig. 7) and is characterized by the increase of cathodic current by 0.1–0.2 mA.

The average values of the current measured during rubbing (I_{rub}) at imposed anodic potential (+0.5 V) and the excess current I_{exc} (difference between I_{rub} and the mean of the current before and after rubbing) are listed in Table 3.

The excess current represents the extent of wear-accelerated corrosion. Therefore, the excess current was set to 0 for PPN-I and PPN-II. In general there is a good repeatability of the results.

The wear track volumes are listed in Table 3. It is interesting to note that the volume loss remains almost constant from cathodic (−1.2 V) to anodic (+0.5 V) potentials for the nitrided samples, while for the untreated CoCrMo alloy there is one order of magnitude increase in volume from cathodic to anodic.

4.4 Dry Tests

The volumes of the wear tracks formed during dry rubbing are listed in Table 4 together with the corresponding COF.

Table 3 Tribocorrosion data obtained for the untreated and treated CoCrMo in 0.9 wt% NaCl

Sample	Potential (V)	I_{rub} (mA)	I_{exc} (mA)	Wear track volume (10^{-2} mm^3)	Wear track depth (μm)	COF
Untreated CoCrMo alloy	−1.2	−0.780	–	0.30	1.35	0.32
	−1.2	−0.470	–	0.35	1.10	0.34
	OCP	–	–	0.49	2.31	0.34
	OCP	–	–	0.50	2.51	0.35
	+0.5	0.132	0.132	3.81	9.16	0.36
	+0.5	0.135	0.129	4.01	9.12	0.40
PPN-I	−1.2	−0.624	–	0.34	2.33	0.31
	−1.2	−0.597	–	0.32	1.71	0.31
	OCP	–	–	0.63	2.31	0.34
	OCP	–	–	0.58	3.05	0.36
	+0.5	0.140	0	0.67	2.89	0.28
	+0.5	0.084	0	0.63	2.87	0.27
PPN-II	−1.2	−0.676	–	0.44	1.61	0.37
	−1.2	−0.665	–	0.35	1.68	0.40
	OCP	–	–	0.72	2.53	0.31
	OCP	–	–	0.93	2.66	0.40
	+0.5	0.474	0	0.79	2.86	0.34
	+0.5	0.535	0	0.67	2.74	0.38

The results of two independent experiments per each testing condition are shown in the table

163

Table 4 Total volume losses and COF after dry tests

	Total volume loss (10^{-2} mm^3)	COF
Untreated CoCrMo alloy	4.10	0.47
	4.74	0.42
PPN-I	0.43	0.31
	0.38	0.31
PPN-II	0.31	0.55
	0.38	0.48

The results of two independent tests per each testing condition are shown in the table

Clearly both nitriding treatments reduce the material removal by one order of magnitude in dry conditions. This observation has been also reported in other tribological studies performed on plasma nitriding of CoCrMo alloys [3–6]. In addition, the PPN-I treatment also reduces friction. It is interesting to note that PPN-II shows the lowest volume loss despite the highest COF.

Interestingly, while nitriding clearly reduces wear in dry conditions, its effect in NaCl is less pronounced. This phenomenon was already observed in previous studies on nitrided CoCrMo [8] and on nitrided NiCr [18] and was related to the different wear mechanisms acting on each material depending on the environment.

4.5 Wear Topography

SEM pictures of selected wear tracks after tribocorrosion and dry tests for all samples are shown in Fig. 8. In general,
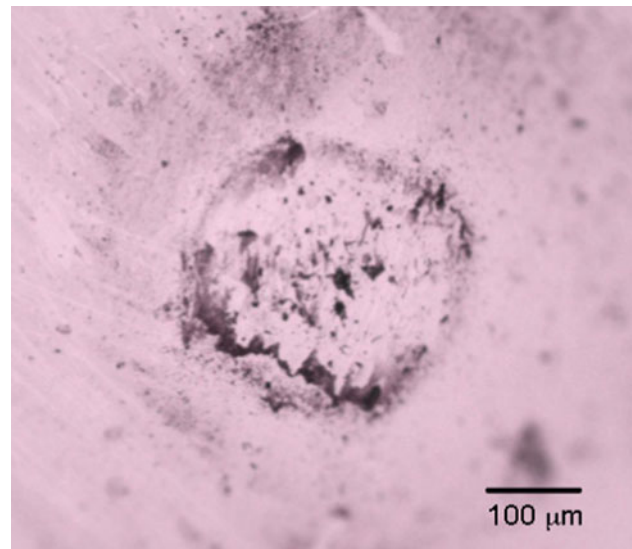

Fig. 9 Optical micrograph of the alumina ball rubbing against PPN-II at +0.5 V

the wear tracks of the nitrided samples appear smooth at all potentials. For the untreated samples, smooth topography is found at the cathodic potential, while at OCP and anodic potential, scratches are observed along the sliding direction. The wear morphology of the treated samples after the dry tests is very similar to the one observed in tribocorrosion tests. However, the untreated alloy exhibits several micrometre-sized large wear debris particles indicating severe wear.
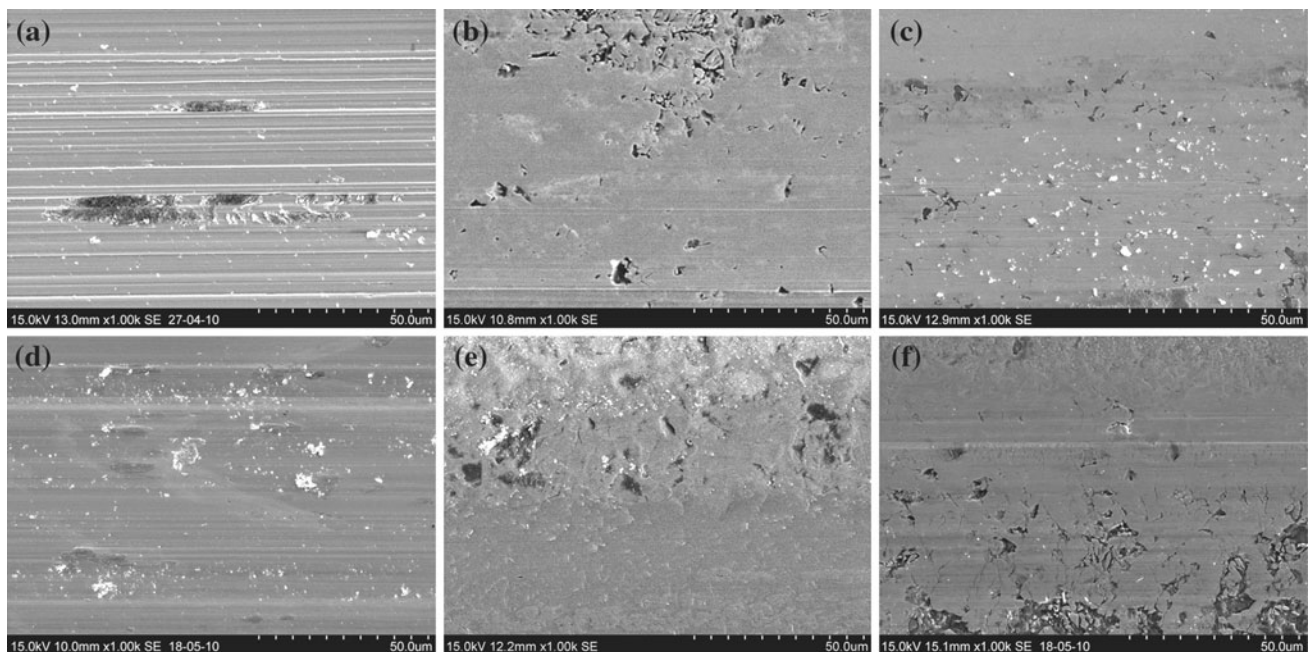

Fig. 8 SEM images of the wear tracks after the tribocorrosion tests of the **a** untreated alloy at +0.5 V, **b** PPN-I at OCP and **c** PPN-II at cathodic potential. Images (**d–f**) show the untreated, PPN-I and PPN-II samples, respectively, after dry tests

Table 5 Co, Cr and Mo ion concentration in solution after the tribocorrosion tests

Sample	Potential (V)	Co (ppm)	Cr (ppm)	Mo (ppm)	%Co ions	%Cr ions	%Mo ions
Untreated CoCrMo alloy	−1.2	0.0277	0.0077	0.0051	68	19	13
	OCP	0.0947	0.0120	0.0030	86	11	3
	+0.5	0.8944	0.1320	0.0376	84	12	3
PPN-I	−1.2	0.0359	0.0047	0.0050	79	10	11
	OCP	0.1074	0.0104	0.0073	86	8	6
	+0.5	0.9264	0.0105	0.0103	98	1	1
PPN-II	−1.2	0.1081	0.0077	0.0053	89	6	4
	OCP	0.8380	0.0289	0.0074	96	3	1
	+0.5	7.7436	0.0250	0.0052	99.6	0.3	0.1

The corresponding percentage in the alloy has been calculated from the solution content and shown in the table

The alumina balls were investigated using optical microscopy to identify possible damage. No alumina wear could be observed, but in all cases some wear debris was found adhering on the contact zone of the ball as shown in Fig. 9.

4.6 ICP-MS Results

Table 5 shows the ion concentrations in the retrieved solutions after tribocorrosion tests. The concentration ratio of Co is always higher than what is expected from the alloy stoichiometry. This can be explained by the fact that Co forms dissolved ions, while Cr rather precipitates as solid oxide. Part of the solid particles remained in the electrochemical cell after pouring the solution, which is thus expected to be enriched in Co. Indeed, debris particles adhering to the metal sample (Fig. 8) and to the ball (Fig. 9) were observed.

5 Discussion

5.1 Contribution of the Different Mechanisms to Overall Degradation

In the present tribocorrosion experiments, different mechanisms were identified, contributing to the overall volume loss: corrosion, wear-accelerated corrosion and mechanical wear. The relevance of each mechanism varied depending on potential and material. Their contribution was quantified using Eqs. 1–3 and taking into account the following assumptions:

- The wear track volume ($V_{\text{wear track}}$) corresponds to the sum of V_{mech} and V_{wac} (Eq. 1).
- In the case of the untreated alloy, V_{wac} was calculated using the I_{exc} (Table 3) and Faraday's law [9]. The nitrided samples are not passive at +0.5 V, and thus

wear-accelerated corrosion is not expected to occur ($V_{\text{wac}} = 0$).
- The corrosion volume (V_{corr}) is negligible at cathodic potentials (insufficient driving force for corrosion) and at +0.5 V for the untreated CoCrMo alloy (passive state).
- At OCP, V_{corr} is calculated using Faraday's law [9] from the i_{corr} values listed in Table 2. Note that the corrosion rates depend on the prevailing electrochemical conditions. In the present study, the potentials established during rubbing (Fig. 5) are very close to the corrosion potentials at which the corrosion rates were measured (Table 2). This lends support to this assumption.
- At +0.5 V for the nitrided samples, V_{corr} is calculated using Faraday's law [9] and the I_{rub} values listed in Table 3.

At OCP, the untreated CoCrMo alloy and the PPN-I are likely passive and thus prone to wear-accelerated corrosion (V_{wac}). However, it is not possible to measure current during the rubbing at OCP, and thus V_{wac} and the mechanical wear (V_{mech}) cannot be determined. According to this, the different volume contributions were calculated and listed in Table 6.

Potential has a marked effect on the wear track volume of the untreated CoCrMo alloy (Fig. 10). This is due not only to the enhancement of wear-accelerated corrosion at high anodic potentials, but also to the dependence of mechanical wear on the established electrochemical conditions (Table 6). Indeed, the presence of a passive film was observed to promote mechanical wear of stainless steels and NiCr alloys [19–22]. This effect was attributed to the influence of passive film on dislocation generation and motion in the underlying metal [19, 21].

On the nitrided samples, the effect of potential on wear track volume is much less pronounced (Fig. 10). The independence of wear on potential can be beneficial for tribocorrosion applications where the electrochemical

Table 6 Volume loss contributions after considering the assumptions for the different electrochemical conditions of the tests

	Potential (V)	V_{mech} (10^{-2} mm^3)	V_{wac} (10^{-2} mm^3)	V_{corr} (10^{-2} mm^3)	$V_{wear\ track}$ (10^{-2} mm^3)	V_{tot} (10^{-2} mm^3)
Untreated CoCrMo alloy	−1.20	0.33	0	0	0.33	0.33
	−0.21[a]	n.d.	n.d.	0.003	0.50	0.50
	+0.50	2.36	1.54	0	3.90	3.90
PPN-I	−1.20	0.33	0	0	0.33	0.33
	−0.01[a]	n.d.	n.d.	0.019	0.61	0.63
	+0.50	0.65	0	1.262	0.65	1.91
PPN-II	−1.20	0.40	0	0	0.40	0.40
	−0.04[a]	n.d.	n.d.	0.004	0.82	0.82
	+0.50	0.73	0	5.794	0.73	6.52

n.d. non determined

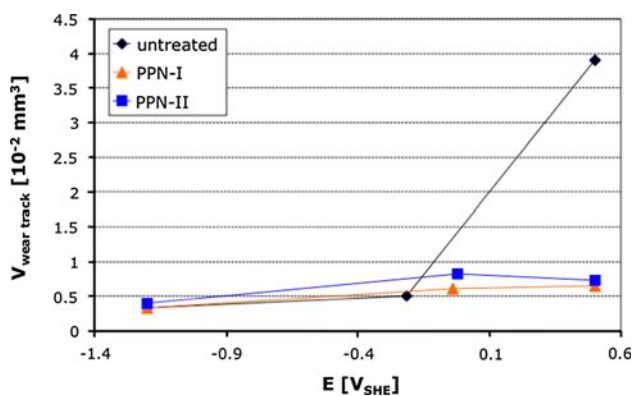[a] Average OCP values during rubbing (Fig. 5)

Fig. 10 Wear track volume as function of potential during tribocorrosion tests

conditions in the contact are unknown or variable. This is, for example, the case of joint prostheses. However, the nitrided samples suffer of severe corrosion on the overall sample surface at higher potential.

This clearly shows that the electrochemical conditions determine the extent by which different mechanisms (corrosion, mechanical wear and wear-accelerated corrosion) influence material degradation. Therefore, materials selection should address the specific degradation mechanisms to be inhibited considering that the potential can trigger severe degradation depending on the acting mechanism.

5.2 Impact of Degradation Mechanisms on Material Release

Figure 11a shows that a linear proportionality exists between the total ion concentration as measured by ICP-MS and the total volume loss from the samples. This is indeed expected as degradation of the materials is the source of dissolved ions in the solution. The fact that the intercepts are negative is probably linked to the wear debris not collected during the retrieval of the electrolyte as explained in Sect. 4.6. This linearity supports the quantification approach taken in this study (Sect. 5.1), which allows also correlating the degradation mechanisms with the type of dissolved ions. Indeed Fig. 11b, c shows that while Cr concentration is proportional to the wear track volume, such linearity is only found for the Co concentration on the untreated alloy but not on the nitrided samples. This clearly shows that Cr release from nitrided samples occurs as a consequence of tribocorrosion in the contact area, while the Co concentration is significantly affected by corrosion occurring on the whole surface. Indeed corrosion (V_{corr}) of the passive CoCrMo alloy is negligible, while the nitrided samples actively corrode in this environment and particularly at +0.5 V (Figs. 3, 6). Co is released through corrosion as well as in the wear track through particle detachment. Thus, its concentration should be proportional to the total material loss (V_{tot}) as indeed found in Fig. 11d.

5.3 Implications for Implants

Materials for implants should ideally have low corrosion and tribocorrosion rates. However, these two phenomena are coupled as they both depend on surface electrochemical reactions and thus on the composition of the materials and the electrolytes. For example, passive films limit the dissolution of the metal over a wide range of potentials, but render the material sensitive to wear-accelerated corrosion and modify its mechanical behaviour. Thus, tribocorrosion rate may vary significantly depending on potential.

On the other hand, the wear rates of non-passive materials, such as the nitrided layers studied in this study, are not significantly affected by the potential. This can be beneficial in tribocorrosion applications, such as the biomedical implants, where the electrochemical conditions are unknown and may change during lifetime. However, non-
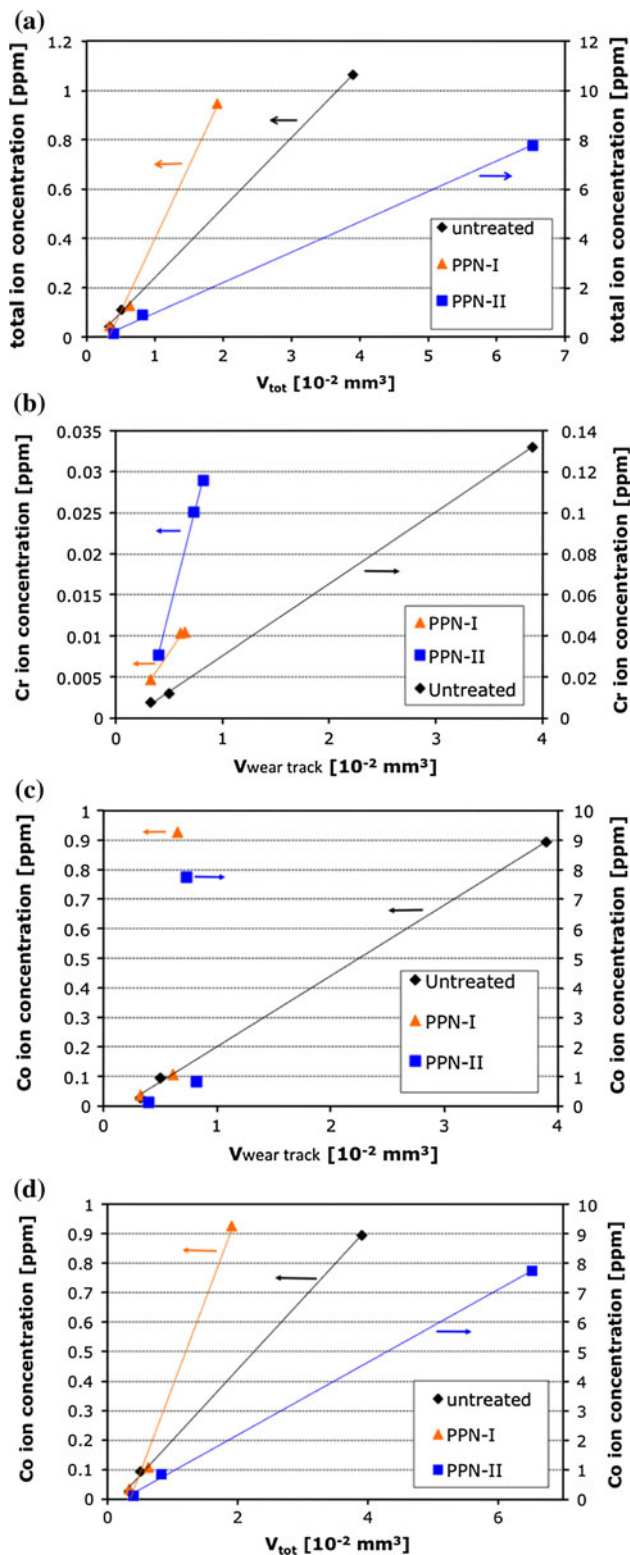
Fig. 11 **a** Total ion concentration plotted versus total volume loss, **b** Cr ion concentration plotted versus wear track volume, **c** Co ion concentration versus wear track volume and **d** Co ion concentration plotted versus total volume loss

passive materials are more sensitive to corrosion especially at higher potentials. Therefore, materials selection should be based on the balance of the different mechanisms contributing to material degradation taking into particular account the electrochemical conditions established in the contact and overall on the implants.

Further critical parameters are the loading, the duty cycle of the implant and its geometry. As an example, at low potentials, the untreated CoCrMo alloy should be preferred to the nitrided samples in the light of its slightly better corrosion and wear performance. However, if the potentials move towards higher values, the nitrided alloy has the advantage of being much less sensitive to increased degradation because of potential changes. However, implant's motion is intermittent and depending on duty cycles, materials can be exposed either to tribocorrosion or only to corrosion. Further, some areas of implants do not experience sliding. Thus, in the latter cases, corrosion resistance becomes a crucial factor in materials selection, and in this respect, the present nitrided materials show some disadvantages that should be overcome with improvements in the nitriding process. In order to achieve this, a sound understanding of the critical parameters and the underlying phenomena needs to be developed.

6 Conclusions

The tribocorrosion of pulsed plasma-nitrided biomedical CoCrMo has been studied in 0.9 wt% NaCl solution. Two different treatment temperatures were used to evaluate the effect of temperature on the final microstructure and on tribocorrosion. The following conclusions can be drawn:

- Composite layers consisting of chromium nitrides dispersed in a nitrogen-enriched metal phase were achieved through pulsed plasma nitriding of a biomedical low carbon CoCrMo alloy. The nitrided alloys exhibit increased hardness (about 800 $HV_{0.1}$) compared with the untreated CoCrMo alloy (400 $HV_{0.1}$), which provides ten times higher wear resistance in dry conditions.
- The formation of the γ_N phase suppresses the passivity of the alloy in 0.9 wt% NaCl and leads to higher corrosion rates at anodic potential. The depletion in Cr due to the formation of chromium nitride seems to play a minor role for corrosion.
- The wear ranking of the materials in 0.9 wt% NaCl depends on the electrochemical conditions. Above a critical potential, the untreated CoCrMo alloy shows very large wear. This is due to its passive nature that promotes wear-accelerated corrosion and mechanical wear. Nitriding suppresses this transition while conferring similar wear rates as found on the untreated CoCrMo alloy at low potentials.

- This study shows that the use of non-passive materials could be beneficial in tribocorrosion applications such as the biomedical ones, as they provide constant wear rates in a wide range of potentials. This is of great importance for selecting the proper material in situations like the human body where the electrochemical conditions are uncontrolled.

References

1. Passuhi, N., Philipeau, J.M., Gouin, F.: Friction couples in total hip replacement. Orthop. Traumatol. **95**(4S), 27–34 (2009)
2. Bauer, T.W.: Particles and periimplant bone resorption. Clin. Orthop. **405**, 138–143 (2002)
3. Wei, R., Booker, T., Rincon, C., Arps, J.: High-intensity plasma ion nitriding of orthopedic materials: Part I. Tribological study. Surf. Coat. Technol. **186**, 305–313 (2004)
4. Lanning, B.R., Wei, R.: High intensity plasma ion nitriding of orthopedic materials: Part II. Microstructural analysis. Surf. Coat. Technol. **186**, 314–319 (2004)
5. Çelik, A., Bayrak, Ö., Alsaran, A., Kaymaz, İ., Yetim, A.F.: Effects of plasma nitriding on mechanical and tribological properties of CoCrMo alloy. Surf. Coat. Technol. **202**, 2433–2438 (2008)
6. Pichon, L., Okur, S., Öztürk, O., Rivière, J.P., Drouet, M.: CoCrMo alloy treated by floating potential plasma assisted nitriding and plasma based ion implantation: influence of the hydrogen content and of the ion energy on the nitrogen incorporation. Surf. Coat. Technol. **204**, 2913–2918 (2010)
7. Öztürk, O., Türkan, U., Eroğlu, A.: Metal ion release from nitrogen ion implanted CoCrMo orthopedic implant material. Surf. Coat. Technol. **200**, 5687–5697 (2006)
8. Lutz, J., Mändl, S.: Reduced tribocorrosion of CoCr alloys in simulated body fluid after nitrogen insertion. Surf. Coat. Technol. **204**, 3043–3046 (2010)
9. Mischler, S.: Triboelectrochemical techniques and interpretation methods in tribocorrosion: a comparative evaluation. Tribol. Int. **41**, 573–583 (2008)
10. Wu, J.: Metallography and Microstructures of Cobalt and Cobalt Alloys, Metallography and Microstructures, vol. 9. ASM Handbook, ASM International, Materials Park, pp. 762–774 (2004)
11. Suegama, P.H., Fugivara, C.S., Benedetti, A.V., Fernández, J., Espallargas, N., Delgado, J., Guilemany, J.M.: Microstructure and electrochemical studies of Cr_3C_2–NiCr coatings obtained by HVOF. In: Vargus, E.P. (ed.) New Researches on Electrochemistry, Chapter 4. Nova Science Publishers, Inc., New York, p. 113 (2007)
12. Azzi, M., Szpunar, J.A.: Tribo-electrochemical technique for studying tribocorrosion behavior of biomaterials. Biomol. Eng. **24**, 443–446 (2007)
13. Green, S.M.: Deformation of materials. Curr. Orthop. **20**, 9–15 (2006)
14. Hodge, W.A., Carlson, K.L., Fijan, R.S., Burgess, R.G., Righley, P.O., Harris, W.H., Mann, R.W.: Contact pressures from an instrumented hip endoprosthesis. J. Bone Jt. Surg. **71**, 1378–1386 (1989)
15. Lutz, J., Gerlach, J.W., Mändl, S.: PIII nitriding of fcc-alloys containing Ni and Cr. Phys. Stat. Solidi (A) **205**(4), 980–984 (2008)
16. Landolt, D.: Corrosion and Surface Chemistry of Metals. EPFL Press, Lausanne (2007)
17. Igual-Muñoz, A., Mischler, S.: Effect of the environment on wear ranking and corrosion of biomedical CoCrMo alloys. J. Mater. Sci. Mater. Med. **22**(3), 437–450 (2011)
18. Espallargas, N., Mischler, S.: Dry wear and tribocorrosion mechanisms of pulsed plasma nitrided Ni–Cr alloy. Wear **270**, 464–471 (2011)
19. Bidiville, A., Favero, M., Stadelmann, P., Mischler, S.: Effect of surface chemistry on the mechanical response of metals in sliding tribocorrosion systems. Wear **263**(1–6), 207–217 (2007)
20. Perret, J., Boehm-Courjault, E., Cantoni, M., Mischler, S.: EBSD, SEM and FIB characterisation of subsurface deformation during tribocorrosion of stainless steel in sulphuric acid. Wear **269**, 383–393 (2010)
21. Favero, M., Stadelmann, P., Mischler, S.: Effect of the applied potential of the near surface microstructure of a 316L steel submitted to tribocorrosion in sulfuric acid. J. Appl. Phys. D **39**(15), 3175–3183 (2006)
22. Espallargas, N., Mischler, S.: Tribocorrosion behaviour of overlay welded Ni–Cr 625 alloy in sulphuric and nitric acids: Electrochemical and chemical effects. Tribol. Int. **43**(7), 1209–1217 (2010)